NANO
LETTERS

xxxx
Vol. 0, No. 0
A−F

Mapping the Plasmon Resonances of Metallic Nanoantennas

Garnett W. Bryant,*,† F. Javier García de Abajo,‡ and Javier Aizpurua§

National Institute of Standards and Technology, Gaithersburg, Maryland 20899-8423, Instituto de Óptica, CSIC, Serrano 121, 28006 Madrid, Spain, and Donostia International Physics Center, Paseo Manuel de Lardizabal 4, 20018 Donostia, Spain

Received November 21, 2007

ABSTRACT

We study the light scattering and surface plasmon resonances of Au nanorods that are commonly used as optical nanoantennas in analogy to dipole radio antennas for chemical and biodetection field-enhanced spectroscopies and scanned-probe microscopies. With the use of the boundary element method, we calculate the nanorod near-field and far-field response to show how the nanorod shape and dimensions determine its optical response. A full mapping of the size (length and radius) dependence for Au nanorods is obtained. The dipolar plasmon resonance wavelength λ shows a nearly linear dependence on total rod length L out to the largest lengths that we study. However, L is always substantially less than $\lambda/2$, indicating the difference between optical nanoantennas and long-wavelength traditional $\lambda/2$ antennas. Although it is often assumed that the plasmon wavelength scales with the nanorod aspect ratio, we find that this scaling does not apply except in the extreme limit of very small, spherical nanoparticles. The plasmon response depends critically on both the rod length and radius. Large (500 nm) differences in resonance wavelength are found for structures with different sizes but with the same aspect ratio. In addition, the plasmon resonance deduced from the near-field enhancement can be significantly red-shifted due to retardation from the resonance in far-field scattering. Large differences in near-field and far-field response, together with the breakdown of the simple scaling law must be accounted for in the choice and design of metallic $\lambda/2$ nanoantennas. We provide a general, practical map of the resonances for use in locating the desired response for gold nanoantennas.

Over the past decade, intense renewed effort has been made to understand the plasmonics of metallic nanoparticles. The ability to tune the plasmon resonances over a wide wavelength range via the choice of nanoparticle size, shape, and composition, extreme local-field enhancements, and intense far-field scattering are all strong motivations for applications in high-resolution and single-molecule microscopy and spectroscopy, surface-enhanced Raman spectroscopy, biosensing, and optical communication below the diffraction limit.[1−14] Explicit control of the plasmon response has been achieved by the use of different particle shapes, such as nanoshells,[15] nanorings,[16] and nanorods.[17] Recently, the analogy between nanorods, acting as nanoantennas with response in the optical regime, and traditional microwave and radio wave antennas has been brought out, explored, and exploited.[18−23] Linear scaling of the plasmon resonance wavelength λ with total nanorod length L emphasizes this analogy. The dipolar mode of such nanoantennas is often referred to as the $\lambda/2$ mode with the expectation that the resonance should occur when L is a half wavelength, as happens for traditional long-wavelength antennas made from nearly perfect conductors with skin depths much less than the antenna size. While such an assignment is tempting, it has not been established and previous simulations[17,22] suggest that it is not the case for nanoantennas where the skin depth is comparable to or much larger than the nanorod dimensions. Thus, it is imperative that a full mapping of the nanorod plasmon be obtained as a function of nanorod size and shape (length L and radius R), both to understand how and when nanoantennas differ from traditional antennas and to provide useful guidelines for nanoantenna design needed for antenna-assisted fluorescence, spectroscopy, and sensing.

Nanorods have been studied theoretically in detail.[17,24−36] However, typically the focus has been to provide an understanding of plasmon resonances in nanostructures by limiting the calculations to specific sizes (typically, particular radii Rs) or limited size ranges. It is well known that in the quasistatic limit, where the light wavelength is much larger than the particle size ($\lambda \gg L, R$), the plasmon resonance should be independent of particle size and depend only on particle shape via the aspect ratio $L/(2R)$. As a consequence, much of the theoretical work has highlighted the dependence of the plasmon resonance on aspect ratio, ignoring any explicit dependence on nanorod length or radius. Because the quasistatic model is simple but intuitively compelling, it has also been used as a simple model for the general

* Corresponding author. E-mail: garnett.bryant@nist.gov.
† National Institute of Standards and Technology.
‡ Instituto de Óptica.
§ Donostia International Physics Center.

10.1021/nl073042v CCC: $40.75
Published on Web 01/12/2008

properties of local plasmons in nanostructures.[37] In this letter, we present a full mapping of the plasmon dipole resonances in Au nanorods, explicitly determining the L and R dependence over the range typical of these nanoparticles ($L < 2000$ nm, $R < 100$ nm). This mapping is obtained from exact electromagnetic calculations. The mapping demonstrates that the plasmon resonance depends linearly on rod length over most of this range of L but with a scaling that differs significantly from the scaling assumed for $\lambda/2$ antennas. Most importantly, our results show how this linear dependence changes as R is increased and retardation effects become important. Finally, with a full mapping we show that the quasistatic limit applies only over a very narrow range of sizes and shapes close to a sphere and that aspect ratio should not be used to describe nanoparticle properties, except in this very limited size regime. Recently, Prescott and Mulvaney[34] reached a similar conclusion about the use of aspect ratio.

The optical response of the nanorods is calculated exactly by means of the boundary element method in a full electromagnetic calculation,[16,17,38,39] including retardation. We consider external light incident normal to the nanorod axis and polarized along the rod. Even though the radius R is at least a factor of 5 smaller than the incident wavelength, our results show that retardation effects across the structures are important and must be included. Maxwell's equations for nanostructures with sharp boundaries are solved in terms of effective surface charges and surface currents. Boundary conditions are imposed via surface integrals along the nanorod boundaries. The metal is characterized by a local bulk dielectric function. The external fields interact self-consistently with the induced surface charges and currents, which are determined by discretizing the surface integrals on a grid on the surface and solving the resulting matrix equations. We calculate in this way the near and far fields for a given structure. In this letter, we focus on Au nanorods. We obtained similar results for other materials. For Au, we use the bulk dielectric function tabulated by Johnson and Christy.[40] We have extended the tabulated results to longer wavelength by matching the tabulated dielectric function to a Drude form at long wavelength using the Drude parameters suggested by Johnson and Christy. In this letter, we consider nanorods consisting of a cylindrical rod, radius R and length L_{rod}, capped with hemispherical ends, radius R, such that the total length $L \equiv L_{tot} = L_{rod} + 2R$ (see Figure 1). In this case, the aspect ratio is $L_{tot}/(2R) = (L_{rod}/(2R)) + 1$.

To define the plasmon resonances, we first calculate the far field in the forward direction, the far-field scattering (i.e., the scattering cross section obtained from the optical theorem) and the near field (normalized to the incident field) one nanometer from the rod end, each as a function of the incident wavelength.[17] The peak in the response at the longest wavelength defines the dipole resonance, which is the lowest-energy, optically active resonance with a single node in the surface charge density. Figure 1 shows a typical surface charge density for the nanorod dipole mode.[17] The charge oscillation is cut off at the rod ends and is less than a half wavelength oscillation. Resonance peaks at shorter wavelengths are assigned to higher-order, optically active resonances. The peak wavelength for the dipolar resonance as a function of total rod length is shown in Figure 2 for Au nanorods with $R = 20$, 50, and 100 nm. In each case, we show the resonance wavelengths as extracted from the far field in the forward direction, the far-field scattering, and the normalized near field. Over the range of L_{tot} shown, the resonance wavelength increases linearly with increasing L_{tot}, except when $L_{tot} \approx 2R$ and end effects are dominant. For $L_{tot} > 800$ nm, the increase becomes slightly sublinear but would not be noticeable in the figures shown here. For small R, dipole resonance wavelengths extracted from the far field,

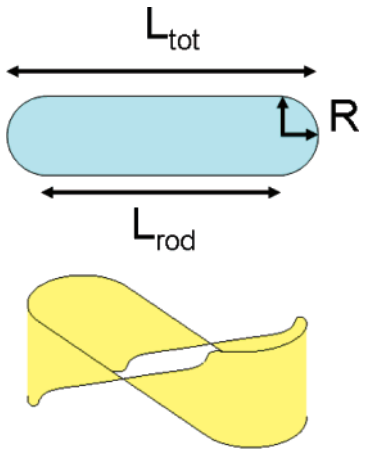

Figure 1. Schematic and dimensions of the cylindrical nanorod with hemispherical caps studied here and the surface charge density typical for a dipolar resonance.

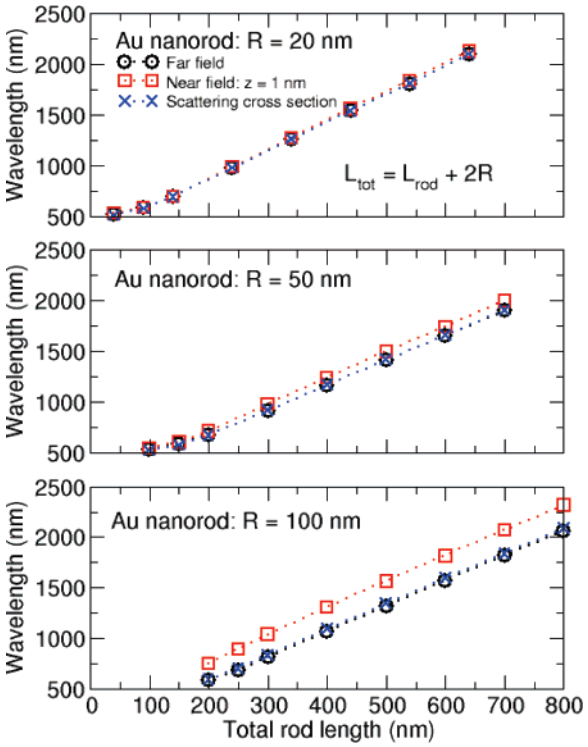

Figure 2. Dependence of the dipolar resonance wavelength on nanorod length for $R = 20$, 50, and 100 nm. The resonance wavelengths extracted from the forward far-field, the far-field scattering, and the normalized near-field are shown.

near field, and far-field scattering are nearly identical. As R increases, the resonances extracted from the forward far-field and far-field scattering remain nearly equal for the range of R studied here. However, the near-field resonance becomes noticeably red-shifted from the far-field resonances for $R =$ 50 nm. For $R = 100$ nm, the red-shift is about 200 nm for the range of rod lengths considered. This shift is comparable to the resonance half-width. This large red-shift could have important implications for the design and optimization of these nanostructures because the resonance wavelength depends substantially on which response is to be engineered. This red-shift between the near-field and far-field responses is a signature of the onset of retardation effects, which become important for rod diameters on the order of one fifth of a wavelength.

The near-field resonance wavelength also depends on where in the near field the response is measured. A blue-shift of the resonance is observed as the near-field position is moved back along the rod from the rod end to the center of the nanorod while remaining a fixed distance away from the nanorod surface. For a large nanorod with $L_{tot} = 400$ nm and $R = 100$ nm, this blue-shift is about 150 nm. For a thinner nanorod with $L_{tot} = 280$ nm and $R = 40$ nm, this blue-shift is about 50 nm. This variation along the rod axis could also be key for any application that exploits the plasmon resonance to modify the response of attached molecules or other nanostructures.

As the nanorod length increases, additional, higher order, optically active resonances appear initially at short wavelengths, near the resonance for a spherical nanoparticle and then red-shift linearly with L_{tot}.[17] For smaller R, the shorter wavelength resonances that appear first for increasing rod length are the higher order, optically active longitudinal resonances (those resonances with odd numbers of nodes in the surface charge density). These higher order resonances show up in both the far-field and near-field response with a smaller red-shift between the far-field and near-field response than for the dipolar resonance. However, for the thickest nanorod we consider here ($R = 100$ nm), the first higher order resonance that occurs with increasing rod length appears to be a transverse mode with strong far-field response and weak near-field response at the rod end. That a mode with response transverse to the rod can be driven by a longitudinal polarization is another signature of the onset of retardation effects with the surface charge on opposite sides of the nanorod being driven by local incident fields with different phases. As the rod length increases, this transverse resonance weakens and disappears because it becomes increasingly more difficult to drive a resonance that has a transverse oscillation with an incident field that has longitudinal polarization. As the transverse resonance weakens, higher order, optically active longitudinal resonances become the dominant higher order resonances.

Intuitively, one would expect that the dipole response at the end of the rod is enhanced by minimizing any excitation of these transverse modes. At points along the rod further away from the rod end, the local response should be enhanced by mixing higher order longitudinal and transverse

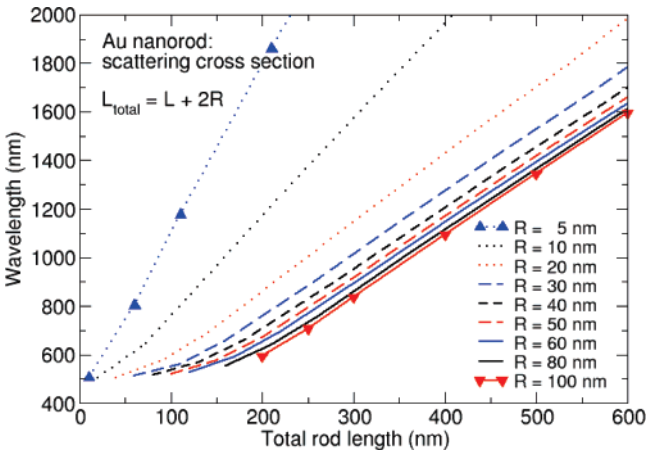

Figure 3. The full dependence of the dipole resonance wavelength on L_{tot} for different R. The resonance wavelength extracted from the far-field scattering is shown.

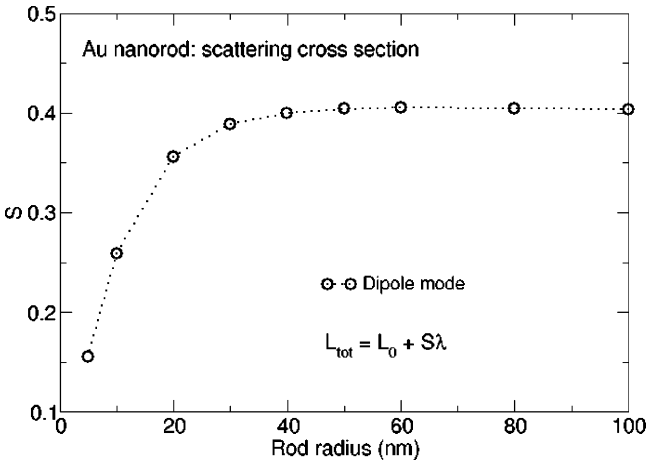

Figure 4. Slope S for the linear dependence between nanorod length and resonant wavelength.

modes. Consequently, the resonance peak for the near-field at the rod end should occur at the longest wavelength, while away from the rod end the mixing should blue-shift the peak response. In addition, the far-field scattering should be enhanced by an appropriate mixture of these modes and should also be blue-shifted from the near-field response at the rod end. Finally, the contribution of the transverse modes excited due to retardation effects should be weaker in thinner rods. Our results support this intuition.

The full dependence of the dipole resonance wavelength on L_{tot} for different R is shown in Figure 3. Here, we show the resonance wavelength extracted from the far-field scattering. The linear dependence on L_{tot}, except for $L_{tot} \approx 2R$, is clear. However, the linear dependence varies substantially with R. The slope S for this linear dependence, defined as $L_{tot} = L_0 + S\lambda$, is shown in Figure 4 as a function of R. A slope $S = 1/2$ would correspond to the linear dependence expected for a half-wavelength antenna made from a perfect conductor. For small R, the nanoantennas are far away from a $\lambda/2$ antenna, indicating that much less than a half-wavelength of surface charge oscillation fits on the nanorod at resonance (as seen in Figure 1). End effects and the effects of the finite skin depth of Au are essential.[22] The skin depth

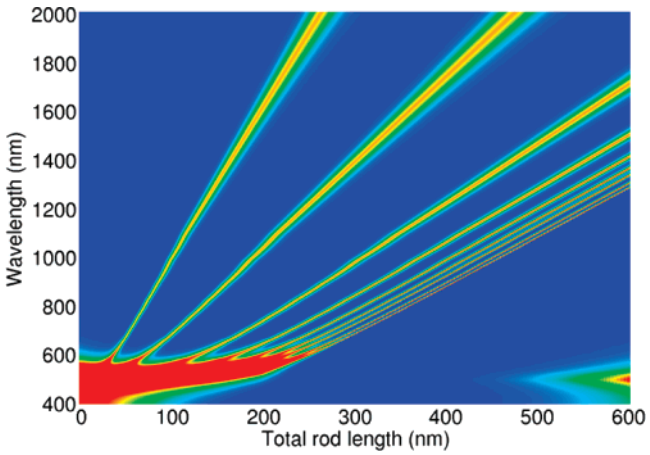

Figure 5. The dependence of the dipole resonance wavelength on L_{tot} for different R as obtained from the folded spectrum of an infinite cylinder (i.e., with the prescription $q = \pi/L_{tot}$ for the longitudinal wavevector). The same values of R are shown here as in Figure 3.

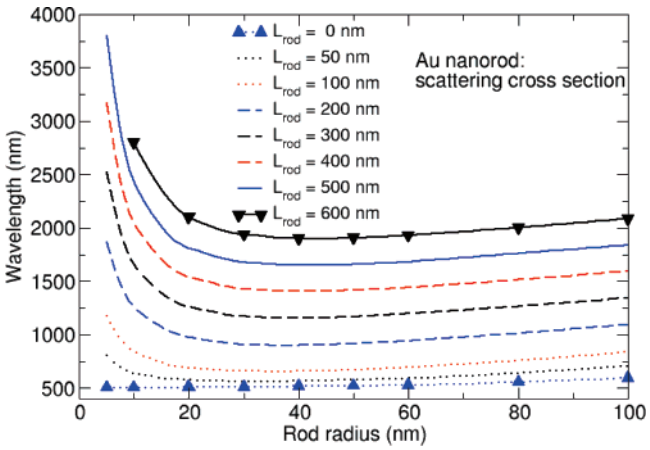

Figure 6. The full dependence of the dipole resonance wavelength on R for different L_{rod}. The resonance wavelength extracted from the far-field scattering is shown.

of Au at these wavelengths is on the order of 20−30 nm. The nanorods are far from perfect conductors because an external field can penetrate across the structure. In addition, for small R the sharp ends should inhibit full charge build-up, suppressing half-wavelength charge oscillations that have peak charge density at the rod ends. As R increases, the slope S monotonically increases, indicating that end effects and the finite skin depth are becoming less significant. However, in the range that we have considered, it appears that the slope has converged to 0.4, still far away from a $\lambda/2$ antenna. In this range, the skin depth is still comparable to the size of the structure. Our results suggest that convergence to the $\lambda/2$ limit will be slow even for micron-sized antennas.

The dipole mode of a nanorod of length L_{tot} and radius R should be related to the plasmon mode with wavevector q for an infinite cylinder with radius R, where $q = \pi/L_{tot}$ (i.e., by relating the nanorod plasmon to the cylinder plasmon that has a half-period of length L_{tot}). Novotny[22] recently considered such a model with an additional R-dependent correction to account for end effects. Using an approximate evaluation, valid for small R, of the dispersion relation for the dipole mode[22,41] and a Drude model for the dielectric function, he found that the dipole resonance wavelength increased linearly with L_{tot} and the slope S increased with R. However, the slopes obtained from his model were higher than those obtained here.

The dispersion relation for the cylindrically symmetric mode of an infinite cylinder is obtained from the dispersion relation,[41] $f = D_r I_0(D_r R)K_1(DR) + \epsilon D I_1(D_r R)K_0(DR) = 0$, where ϵ is the dielectric function of the nanorod, $D = (q^2 - k^2)^{1/2}$, $D_r = (q^2 - \epsilon k^2)^{1/2}$, I_n and K_n are the modified Bessel functions of order n, and $k = 2\pi/\lambda$. To identify the solutions to this dispersion relation, we consider the quantity $1/|f|$,[4] normalized to the maximum value for each lambda (the maximum value is finite because the imaginary part of ϵ broadens the resonance). We sum the contributions from nanorods with the radii as used in Figure 3 and show the dependence on L_{tot} and λ as a contour plot in Figure 5. The resonance wavelengths are identified as maxima at each L_{tot}. We use the dielectric function of Johnson and Christy and evaluate the dispersion exactly for all R. We find a linear dependence of the resonance wavelength on L_{tot} for each R. The slope S for this dependence increases with increasing R. However, the resonance wavelengths obtained from the dispersion relation are significantly shorter than those we obtained for nanorods, as can be seen by comparing Figures 3 and 5. Moreover, the slopes S obtained from the dispersion relation are significantly higher than those in Figure 4. For example, from the dispersion relation, $S = 0.17$, 0.29, and 0.42 for $R = 5$, 10, and 20 nm and for large R, S approaches the expected 1/2 limit. While the simple cylinder model is suggestive, end effects clearly play a crucial role in defining the resonance position. Moreover, similar slopes S are found by Novotny,[22] even when end effects are included in the cylinder model. These simple models predict resonance wavelengths substantially shorter than those we obtain for nanorods. Moreover, the nanorods never reach the $\lambda/2$ limit for the range of R that we consider, while the simpler cylinder models are nearly converged to this limit for $R =$ 100 nm.

The R dependence of the plasmon dipole resonance is shown in Figure 6. This is the same data shown in Figure 3, replotted to highlight the R dependence. The individual curves are for fixed L_{rod}. We plot for fixed L_{rod} so that each curve shows the variation in resonance wavelength as the transverse dimension is scaled. As expected, for spherical particles ($L_{rod} = 0$) the plasmon dipole resonance wavelength increases weakly, red-shifting with increasing particle size due to retardation. For nanorods with finite L_{rod}, two regimes are apparent. At small R, the resonance varies inversely with R, blue-shifting with increasing R, as would be expected for the quasistatic limit where the resonance depends only on the aspect ratio. In contrast, for larger R the resonance increases monotonically at fixed L_{rod}, red-shifting for increasing R as for spherical particles. A similar red-shift is seen for all L_{rod}. The most significant difference for different L_{rod} is that the onset of this retardation effect occurs at larger R for longer nanorods.

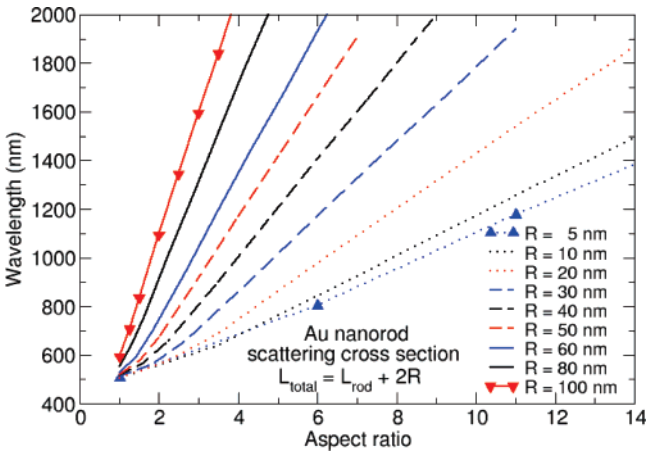

Figure 7. The dependence of the dipole resonance wavelength on aspect ratio $L_{tot}/(2R)$ for different R. The resonance wavelength extracted from the far-field scattering is shown.

So far we have considered the explicit dependence of the plasmon resonance on size and shape by mapping the dependence on both L_{tot} and R. However, it is still common in the literature to highlight the dependence on shape alone under the assumption that nanoparticles are in the quasistatic limit where the resonance depends only on the aspect ratio. In Figure 7, we plot our results as a function of aspect ratio. Each curve corresponds to a fixed R. In the quasistatic limit, where aspect ratio is a meaningful parameter to characterize the structures, the plasmon resonance should be independent of the size (i.e., independent of R) and all curves should lie on a common universal curve. Surprisingly, there is no region, except for the very smallest nearly spherical nanoparticles, where the curves for different R are close. We do not observe scaling with the aspect ratio. For example, the plasmon resonance red-shifts by more than 500 nm in the range of R from 5 to 100 nm for an aspect ratio of only 2. For large aspect ratios, the red-shifts are even larger. These results show that the requirement that the radius be much less than the wavelength really is a stringent requirement, and that outside of this restricted range the quasistatic approximation is limited (see also ref 34). Therefore, the resonance map presented here should be valuable as a practical guide to locating plasmon resonances when designing realizable nanoantennas for molecular fluorescence and spectroscopy.

In conclusion, we have provided a full mapping of the size and shape dependence of the dipolar plasmon resonance of Au nanorods. The dipolar resonance wavelength λ shows a nearly linear dependence on rod length L_{tot} except for small L_{tot}, where the nanorod is nearly spherical and end effects are more important. However, L_{tot} is always substantially less than $\lambda/2$, indicating a key difference between optical nanoantennas and long wavelength, traditional $\lambda/2$ antennas made from nearly perfect conductors. The $\lambda/2$ limit is approached as the nanorod increases in size. However, this limit is not reached on the nanoscale for optical nanoantennas. Although it is often assumed that the plasmon wavelength scales with the nanorod aspect ratio, we find that scaling with the aspect ratio does not apply except in the extreme limit of very small nearly spherical nanoparticles. For small rod radii, the plasmon response blue-shifts with increasing radii and fixed rod cylinder length L_{rod}, as would be expected for scaling with the aspect ratio. However, the plasmon response still depends on both the rod length and radius and does not scale with the aspect ratio. For larger radii, the resonance red-shifts for increasing R and fixed L_{rod}. Moreover, for larger radii the plasmon resonances deduced from the near-field enhancement is significantly red-shifted due to retardation from the resonance in far-field scattering. Such large differences in near-field and far-field response and the breakdown of the simple scaling law must be accounted for in choosing and designing nanoparticles for a particular response.

References

(1) Kneipp, K.; Wang, Y.; Kneipp, H.; Perelman, L. T.; Itzkan, I.; Dasari, R. R.; Feld, M. S. *Phys. Rev. Lett.* **1997**, *78*, 1667.
(2) Knoll, B.; Keilmann, F. *Nature* **1999**, *399*, 134.
(3) Jackson, J. B.; Westcott, S. L.; Hirsch, L. R.; West, J. L.; Halas, N. *Appl. Phys. Lett.* **2003**, *82*, 257.
(4) Talley, C. E.; Jackson, J. B.; Oubre, C.; Grady, N. K.; Hollars, C. W.; Lane, S. M.; Huser, T. R.; Nordlander, P.; Halas, N. *Nano Lett.* **2005**, *5*, 1569.
(5) Félidj, N.; Aubard, J.; Lévi, G.; Krenn, J. R.; Salerno, M.; Schider, G.; Lambrecht, B.; Leitner, A.; Aussenegg, F. R. *Phys. Rev. B* **2002**, *65*, 075419.
(6) Schider, G.; Krenn, J. R.; Hohenau, A.; Ditlbacher, H.; Leitner, A.; Aussenegg, F. R.; Schaich, W. L.; Puscasu, I.; Monacelli, B.; Boreman, G. *Phys. Rev. B* **2003**, *68*, 155427.
(7) Link, S.; El-Sayed, M. A. *J. Phys. Chem. B* **1999**, *103*, 8410.
(8) Lee, K.-S.; El-Sayed, M. A. *J. Phys. Chem. B* **2006**, *110*, 19220.
(9) Xu, H.; Käll, M. *Phys. Rev. Lett.* **2002**, *89*, 246802.
(10) Quinten, M.; Leitner, A.; Krenn, J. R.; Assenegg, F. R. *Opt. Lett.* **1998**, *23*, 1331.
(11) Brongersma, M. L.; Hartman, J. W.; Atwater, H. A. *Phys. Rev. B* **2000**, *62*, 16356.
(12) Maier, S. A.; Kik, P. G.; Atwater, H. A.; Meltzer, S.; Harel, E.; Koel, B. E.; Requicha, A. A. G. *Nat. Mater.* **2003**, *2*, 229.
(13) Jana, N. R.; Gearheart, L.; Murphy, C. J. *J. Phys. Chem. B* **2001**, *105*, 4065.
(14) Stone, J. W.; Sisco, P. N.; Goldsmith, E. C.; Baxter, S. C.; Murphy, C. J. *Nano Lett.* **2007**, *7*, 116.
(15) (a) Averitt, R. D.; Westcott, S. L.; Halas, N. *J. Opt. Soc. Am. B* **1999**, *16*, 1814. (b) Averitt, R. D.; Westcott, S. L.; Halas, N. *J. Opt. Soc. Am. B* **1999**, *16*, 1824.
(16) Aizpurua, J.; Hanarp, P.; Sutherland, D. S.; Käll, M.; Bryant, G. W.; García de Abajo, F. J. *Phys. Rev. Lett.* **2003**, *90*, 057401.
(17) Aizpurua, J.; Bryant, G. W.; Richter, L. J.; García de Abajo, F. J.; Kelly, B. K.; Mallouk, T. *Phys. Rev. B* **2005**, *71*, 235420.
(18) Mühlschlegel, P.; Eisler, H.-J.; Martin, O. J. F.; Hecht, B.; Pohl, D. W. *Science* **2005**, *308*, 1607.
(19) Neubrech, F.; Kolb, T.; Lovrincic, R.; Fahsold, G.; Pucci, A.; Aizpurua, J.; Cornelius, T. W.; Toimil-Molares, M. E.; Neumann, R.; Karim, S. *Appl. Phys. Lett.* **2006**, *89*, 253104.
(20) Cubukcu, E.; Kort, E. A.; Crozier, K. B.; Capasso, F. *Appl. Phys. Lett.* **2006**, *89*, 093120.
(21) Taminiau, T. H.; Moerland, R. J.; Segerink, F. B.; Kuipers, L.; van Hulst, N. F. *Nano Lett.* **2007**, *7*, 28.
(22) Novotny, L. *Phys. Rev. Lett.* **2007**, *98*, 266802.
(23) Muskens, O. L.; Giannini, V.; Sánchez-Gil, J. A.; Gómez Rivas, J. *Nano Lett.* **2007**, *7*, 2871.
(24) Link, S.; Mohamed, M. B.; El-Sayed, M. A. *J. Phys. Chem. B* **1999**, *103*, 3073.
(25) Eustis, S.; El-Sayed, M. A. *J. Phys. Chem. B* **2005**, *109*, 16350.
(26) Eustis, S.; El-Sayed, M. A. *J. App. Phys.* **2006**, *100*, 44324.
(27) Lee, K.-S.; El-Sayed, M. A. *J. Phys. Chem. B* **2005**, *109*, 20331.
(28) Jain, P. K.; Lee, K.-S.; El-Sayed, I. H.; El-Sayed, M. A. *J. Phys. Chem. B* **2006**, *110*, 7238.
(29) Lee, K.-S.; El-Sayed, M. A. *J. Phys. Chem. B* **2006**, *110*, 19220.
(30) Hao, E.; Schatz, G. C. *J. Chem. Phys.* **2004**, *120*, 357.
(31) Payne, E. K.; Shuford, K. L.; Park, S.; Schatz, G. C.; Mirkin, C. A. *J. Phys. Chem. B* **2006**, *110*, 2150.

(32) Brioude, A.; Jiang, X. C.; Pileni, M. P. *J. Phys. Chem. B* **2005**, *109*, 13138.
(33) Sburlan, S. E.; Blanco, L. A.; Neito-Vesperinas, M. *Phys. Rev. B* **2006**, *73*, 035403.
(34) Prescott, S. W.; Mulvaney, P. *J. Appl. Phys.* **2006**, *99*, 123504.
(35) Noguez, C. *J. Phys. Chem. C* **2007**, *111*, 3806.
(36) Khlebtsov, B. N.; Khlebtsov, N. G. *J. Phys. Chem. C* **2007**, *111*, 11516.
(37) Wang, F.; Shen, Y. R. *Phys. Rev. Lett.* **2006**, *97*, 206806.
(38) (a) García de Abajo, F. J.; Howie, A. *Phys. Rev. Lett.* **1998**, *80*, 5180. (b) García de Abajo, F. J.; Howie, A. *Phys. Rev. B* **2002**, *65*, 115418.
(39) Romero, I.; Aizpurua, J.; Bryant, G. W.; García de Abajo, F. J. *Opt. Express* **2006**, *14*, 9988.
(40) Johnson, P. B.; Christy, R. W. *Phys. Rev. B* **1972**, *6*, 4370.
(41) Ashley, J. C.; Emerson, L. C. *Surf. Sci.* **1974**, *41*, 615.

NL073042V